World Academy of Science, Engineering and Technology
International Journal of Chemical and Molecular Engineering
Vol:8, No:11, 2014

Numerical Comparison of Rushton Turbine and CD-6 Impeller in Non-Newtonian Fluid Stirred Tank

Akhilesh Khapre, Basudeb Munshi

***Abstract*—**A computational fluid dynamics simulation is done for non-Newtonian fluid in a baffled stirred tank. The CMC solution is taken as non-Newtonian shear thinning fluid for simulation. The Reynolds Average Navier Stocks equation with steady state multi reference frame approach is used to simulate flow in the stirred tank. The turbulent flow field is modelled using realizable k-ε turbulence model. The simulated velocity profiles of Rushton turbine is validated with literature data. Then, the simulated flow field of CD-6 impeller is compared with the Rushton turbine. The flow field generated by CD-6 impeller is less in magnitude than the Rushton turbine. The impeller global parameter, power number and flow number, and entropy generation due to viscous dissipation rate is also reported.

***Keywords*—**Computational fluid dynamics, non-Newtonian, Rushton turbine, CD-6 impeller, power number, flow number, viscous dissipation rate.

I. Introduction

MECHANICALLY agitated stirred tanks have been widely used in the chemical, biochemical and pharmaceutical industries [1]. The performance of stirred tank depends on appropriate adjustment of the reactor hardware and operating parameters like a tank and impeller geometry, rotational speed and location of fluid addition and subtraction. Therefore, a detailed knowledge of velocity distribution and power requirement of the stirred tank configuration is required [2].

Over the past year, many researches have been carried out to understand the hydrodynamics behaviour of non-Newtonian fluid inside the stirred tank using experiments and simulations [3]-[10]. The most of the work reported is carried out in laminar and early transition regime of the flow to study power consumption of impeller and cavern size around the impeller. A very few literature is available for turbulent mixing of non-Newtonian fluid. Venneker et al. [6] have reported LDA (Laser Doppler Anemometry) measurements of the turbulent velocity flow fields for non-Newtonian fluids in vessels stirred by a Rushton turbine. They have studied Reynolds number similarity for different non-Newtonian fluids with flow behaviour indices varying from 0.56 to 1. Wu [11] has performed CFD simulation of non-Newtonian fluids in a lab-scale anaerobic digestion tank with a pitched blade turbine (PBT) impeller in the turbulent flow regime. The six turbulence models are used, but realizable k-ε and the standard k-ω models are found to be more suitable than the other turbulence models.

Nowadays, the power consumption is widely recognized as the most important design parameter in mixing application. Although, the mixing of fluid is greatly depends upon the importance of flow patterns and mixing time. Many researchers have shown experimentally and numerically that the power consumption is strongly depended upon the system geometry, type of impeller, the rheological characteristics of the fluid and the kinematic conditions predominant in the tank [2], [12]-[16]. The impeller transfers the power to the fluid near the impeller swept volume, which accounts for the viscous loss due to fluid friction. Hence, study of viscous dissipation rate is important to understand the power consumption. Naterer and Adeyinka [17] studied experimentally the entropy production due to viscous dissipation in laminar fluid motion induced by a magnetic stirrer in a cube tank using particle image velocimetry. They found that the highest rate of entropy production is near the impeller. Driss et al. [18] studied the hydrodynamics and mixing performance of a stirred tank reactor to show the effect of multiple Rushton turbine configurations on the mixing performance. The experimental results were compared with CFD code to getting insight into the viscous dissipation rate. They observed a maximum viscous dissipation rate near the blade tip and a rapid decrease of it towards the tank wall.

In this paper, the hydrodynamic characteristic of non-Newtonian fluid with Rushton turbine and CD-6 impeller in baffled stirred tank at fully turbulent flow regime is predicted using CFD simulation. The simulated velocity distribution profile of Rushton turbine is validated with literature data [6]. The comparative study of local (local velocity components) and global quantities (power number, flow number) for both the impeller is carried out. The entropy generation due to viscous dissipation rate, which gives insight the loss due to power consumption, is also computed.

II. Numerical Details

A. Geometry Specification

The diameter (T) of stirred tank is 0.627m and height (H) of tank is same as that of the diameter of tank as shown in Fig. 1. The diameter of both impeller (D) is $T/3$ and is placed at clearance of $C_i = D$ from bottom wall. Both the impellers have six blades. The four baffles of width (W_b) $1/10^{th}$ of the

Akhilesh Khapre is with National Institute of Technology, Rourkela, Orissa, 769008, India (corresponding author phone: +91-7894044869; e-mail: akhilesh_khapre@yahoo.co.in).

Basudeb Munshi is with National Institute of Technology, Rourkela, Orissa, 769008, India.

diameter of tank are placed along the wall at 90° apart from each other. The shear thinning non-Newtonian fluid used for simulation has rheological property as consistency index (K) is 0.0132 kg•s^{n-2}•m^{-1} and the flow behavior index (n) is 0.85. The temperature of stirred tank is kept constant at 298K.

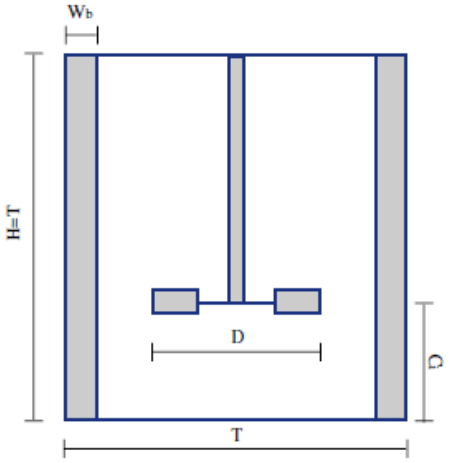

Fig. 2 Geometry of stirred tank [6]

B. Governing Equations and Solver Details

The governing equation of continuity can be written as follows [19],

$$\frac{\partial \rho}{\partial t} + \nabla .(\rho \vec{v}) = 0 \tag{1}$$

where, $\vec{v}$ is the velocity vector.

The conservation of momentum is given by [19]

$$\frac{\partial}{\partial t}(\rho \vec{v}) + \nabla .(\rho \vec{v}\vec{v}) = -\nabla p + \nabla .(\bar{\bar{\tau}}) + \rho \vec{g} \tag{2}$$

where, p is the static pressure and $\bar{\bar{\tau}}$ is the stress tensor; $\vec{g}$ is the gravitational body force. The stress tensor $\bar{\bar{\tau}}$ is given by

$$\bar{\bar{\tau}} = \eta \left[\left(\nabla \vec{v} + \nabla \vec{v}^{T} \right) - \frac{2}{3} \nabla .\vec{v} I \right] \tag{3}$$

where, η is the apparent viscosity, I is the unit tensor.

The two-equation, k-ε model, is used for turbulence modeling in stirred tank. There are three k-ε model available such as standard, RNG and realizable. For this study realizable model k-ε model is used due to its better prediction of spreading rate of jets which are discharging from impeller blades [20]. The two equations that need to be solved for the k-ε model are the turbulence kinetic energy, k, and its rate of dissipation, ε, and those are calculated by the equations [19],

$$\frac{\partial}{\partial t}(\rho k) + \nabla \cdot (\rho k \vec{v}) = \nabla \cdot \left[\left(\eta + \frac{\mu_t}{\sigma_k} \right) \nabla \cdot k \right] + G_k - \rho \varepsilon \tag{4}$$

$$\frac{\partial}{\partial t}(\rho \varepsilon) + \nabla \cdot (\rho \varepsilon \vec{v}) = \nabla \cdot \left[\left(\eta + \frac{\mu_t}{\sigma_\varepsilon} \right) \nabla \cdot \varepsilon \right] + C_{1\varepsilon} \frac{\varepsilon}{k} G_k - C_{2\varepsilon} \rho \frac{\varepsilon^2}{k} \tag{5}$$

The model constant $C_{1\varepsilon}$, $C_{2\varepsilon}$, C_μ, σ_k and σ_ε have the following default values,

$$C_{1\varepsilon} = 1.44, C_{2\varepsilon} = 1.92, C_\mu = 0.09, \sigma_k = 1.0, \sigma_\varepsilon = 1.2$$

The term G_k represents generation of turbulent kinetic energy due to mean velocity gradients and calculated as

$$G_k = -\rho \overline{u_i' u_j'} \frac{\partial u_j}{\partial x_i} \tag{6}$$

The turbulent or eddy viscosity, μ_t, is computed by combining k and ε as follows,

$$\mu_t = \rho C_\mu \frac{k^2}{\varepsilon} \tag{7}$$

For non-Newtonian fluid, the power law is used to model viscosity, is given as

$$\eta = K \dot{\gamma}^{n-1} \tag{8}$$

where, η is apparent viscosity, K is consistency index, n is flow index and $\dot{\gamma}$ is average shear rate

The Reynolds number for shear thinning fluid is calculated using the Metzner-Otto method [21],

$$Re = \frac{\rho N^{2-n} D^2}{K k_s^{n-1}} \tag{9}$$

where, k_s is Metzner-Otto constant.

The power number for impeller is calculated as

$$N_P = \frac{P}{\rho N^3 D^5} \tag{10}$$

where, P is power consumption.

The flow number of impeller is determined using equation

$$N_q = \frac{Q}{ND^3} \tag{11}$$

where, Q is volumetric discharge from impeller blade.

Entropy generation is an important parameter for designing process equipment. Total entropy generation per unit volume is sum of entropy production due to heat transfer and viscous dissipation per unit volume. But in isothermal condition, the entropy production due to temperature gradient i.e. heat transfer is zero. Thus the total entropy generation is completely depended on viscous dissipation rate. The viscous dissipation rate is consisting of mean and fluctuating viscous

dissipation terms due to turbulence. Hence the total entropy generation is given as [22]

$$\dot{S}_{gen} = \frac{\mu_{eff}\varphi_v}{T} + \frac{\rho\varepsilon}{T} \quad (12)$$

The μ_{eff} is the effective viscosity, T is the temperature of system and φ_v is the mean viscous dissipation due to mean velocity components and $\rho\varepsilon$ is fluctuating dissipation due to fluctuating velocity components which are given as

$$\varphi_v = 2\left[\left(\frac{\partial u}{\partial r}\right)^2 + \left(\frac{\partial v}{r\partial\theta} + \frac{u}{r}\right)^2 + \left(\frac{\partial w}{\partial z}\right)^2\right] + \left[\frac{\partial v}{\partial r} - \frac{v}{r} + \frac{\partial u}{r\partial\theta}\right]^2 + \left[\frac{\partial w}{r\partial\theta} + \frac{\partial v}{\partial z}\right]^2 + \left[\frac{\partial u}{\partial z} + \frac{\partial w}{\partial r}\right]^2 \quad (13)$$

$$\rho\varepsilon = 2\left[\overline{\left(\frac{\partial u'}{\partial r}\right)^2} + \overline{\left(\frac{\partial v'}{r\partial\theta} + \frac{u'}{r}\right)^2} + \overline{\left(\frac{\partial w'}{\partial z}\right)^2}\right] + \overline{\left[\frac{\partial v'}{\partial r} - \frac{v'}{r} + \frac{\partial u'}{r\partial\theta}\right]^2} + \overline{\left[\frac{\partial w'}{r\partial\theta} + \frac{\partial v'}{\partial z}\right]^2} + \overline{\left[\frac{\partial u'}{\partial z} + \frac{\partial w'}{\partial r}\right]^2} \quad (14)$$

The ε term in above equation cannot be determined exactly; hence it is replaced with ε-model equation of k-ε turbulence model [23].

C. CFD Solution Procedure

The steady state simulation is carried out using commercial CFD software, Ansys-Fluent 13. The computational domain of stirred tank is discretized into unstructured tetrahedral mesh elements. The mesh independence is carried out by increasing the mesh elements near the impeller and the tank wall. After approximately 900000 mesh elements, the increase in mesh elements did not show more than 5% change in the velocity profile. Thus, the 900000 mesh element is used for further simulation. A steady state multi reference frame (MRF) approach is used for rotation of the impeller. In this approach, a rotating frame is consisted of the impeller and it rotates with the motion of impeller, but the impeller remains stationary. A stationary frame is used for the tank wall and baffles. The momentum equation inside rotating frame is solved in rotating frame, while outside the rotating frame is solved in the stationary frame. Both frames are connected using interface over which a flow properties such as velocity, pressure etc. are exchanged. The mesh element near the impeller region is very fine to capture the dynamics of fluid flow. The inflation layer mesh is created near the wall of tank to resolve a boundary layer. A rotating boundary condition is applied on the shaft which is outside the MRF region and the stationary boundary condition is on the wall of the tank and baffles.

For solving the governing equations numerically, the finite volume method is used for the discretization. The momentum and turbulent transport equation is discretized using second order upwind differencing scheme which offered better accuracy than first order upwind differencing scheme. The result of this process gave a finite set of the coupled algebraic equations which are needed to be solved simultaneously in each grid element in the solution domain. Thus an iterative solution approach is required and is carried out using a Gauss-Seidel iterative method. The SIMPLE (Semi Implicit Method for Pressure Linked Equations) method is applied to linked pressure velocity equation [24]. The non-Newtonian power law is employed to model shear thinning non-Newtonian fluid behavior inside the tank. The convergence criteria are specific conditions for the discretized equation that determines when iterative solution is converged. In this study, the convergence criteria for all discretized equation are set to 10^{-5}.

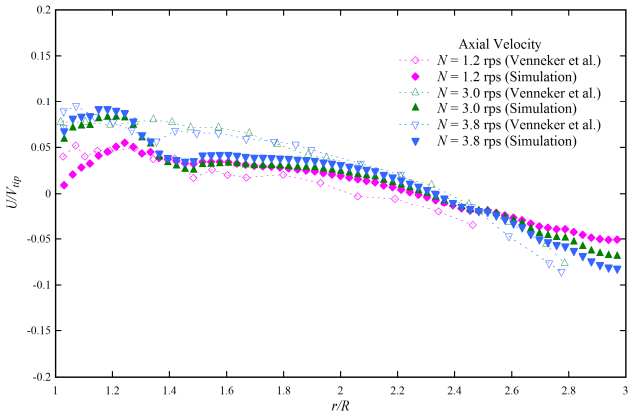

(a) Axial velocity

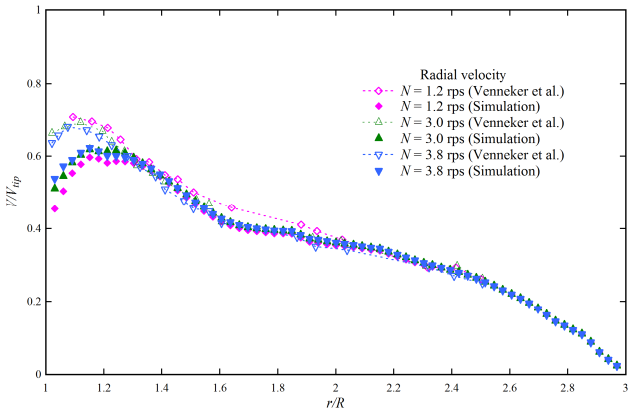

(b) Radial velocity

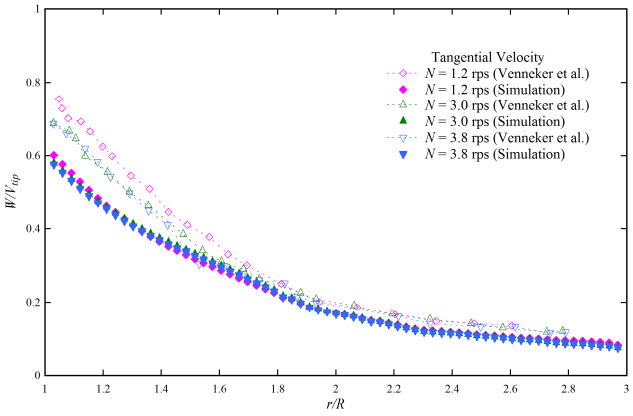

(c) Tangential velocity

Fig. 2 Comparison predicted velocity profile of Rushton turbine with literature data [6]

III. Results and Discussion

The stirred tank with Rushton turbine and CD-6 impeller is simulated for different impeller rotation speeds, N equal to 1.2, 3 and 3.8 rps. The Reynolds number of these rotation speed is calculated using (9) and corresponded to 5900, 16900 and 22200 respectively.

The simulated velocity distribution profiles of Rushton turbine are compared with the literature [6]. The velocity component is normalized using impeller tip velocity, $V_{tip} = \pi ND$. The velocity profiles are taken at the impeller disk level i.e., $H = 0.209$ m, along the dimensionless radial direction, r/R, where r is radial position and R is radius of the impeller. The simulated axial profile shows discrepancy with literature data (Fig. 2 (a)). For $N = 1.2$ rps, the axial profile over predicts with available data. While for remaining rotation speed it under predicts the axial velocity data. Near the impeller blade, the predicted axial velocity approximately matches with the literature value. From Figs. 2 (b) and (c), the predicted radial and tangential velocity component show good agreement with the literature data except near the impeller blade region. At high impeller rotation, the predicted radial and tangential velocity components are almost coinciding with each other. Thus from these observations it can be concluded that the mixing of shear thinning fluid at the turbulent flow regime is largely depending on the axial velocity component.

Fig. 3 shows the velocity vector plots for Rushton turbine and CD-6 impeller at $N = 3$ rps. Both the impellers form two circulation flow pattern, a below and above the impeller disk level. The discharge angle of impinges jets from both the impellers are above the impeller horizontal axis. However the discharge angle of jet from CD-6 impeller is lesser than the Rushton turbine. The Rushton turbine forms larger and more intense circulation loops than CD-6 impeller.

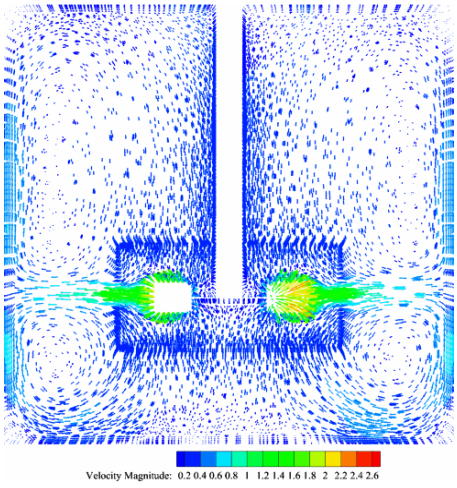

(a) Rushton turbine

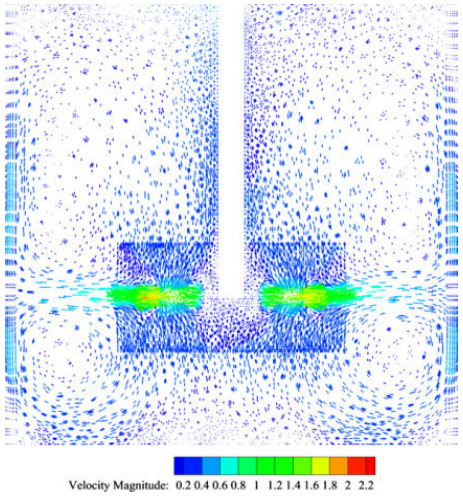

(b) CD-6 impeller

Fig. 3 Velocity vector plots

Fig. 4 shows the comparison of predicted velocity components of CD-6 and Rushton turbine impeller. For all direction velocity profile, the predicted velocities of CD-6 have less magnitude than the Rushton turbine. In Fig. 4 (a), the CD-6 impeller shows negative velocities near the impeller blade. This occurs due to the fluid drawn from the above circulation loop and the fluid which is discharged from the blade of CD-6. Thus, the pick in axial velocity of CD-6 impeller have lower magnitude than the Rushton turbine, this justifies the lesser angle of discharge in Fig. 3. In Fig. 4 (b), the predicted tip velocity of CD-6 is greater than the value of Rushton turbine. But in the bulk area of tank, the velocity magnitude of CD-6 is lower than the Rushton turbine. In Fig. 4 (c), the tangential velocity magnitude of CD-6 impeller is lower than Rushton turbine at impeller disk level. The radial and tangential velocity profiles of CD-6 impeller follow the respective Rushton turbine profile. As the impeller rotation increases, the CD-6 impeller radial and tangential velocity profiles also coincide with each other. Hence, the mixing in CD-6 impeller in turbulence regime also shows dependency only on axial velocity.

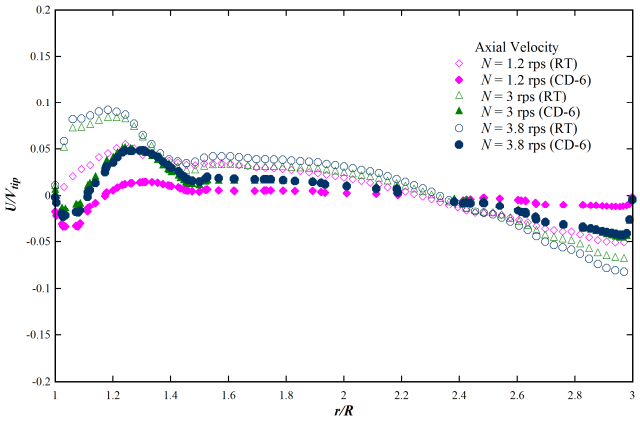

(a) Axial velocity

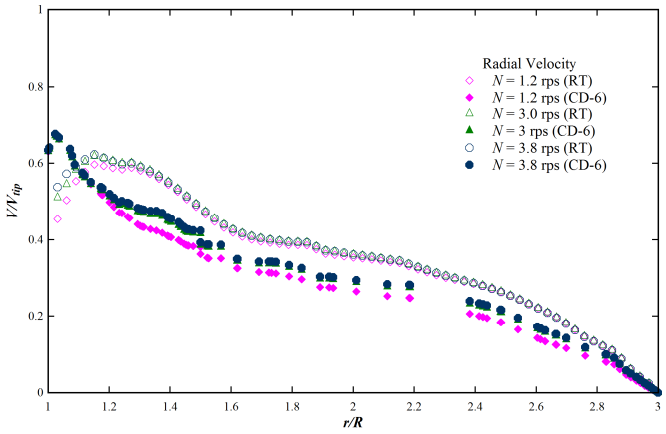

(b) Radial velocity

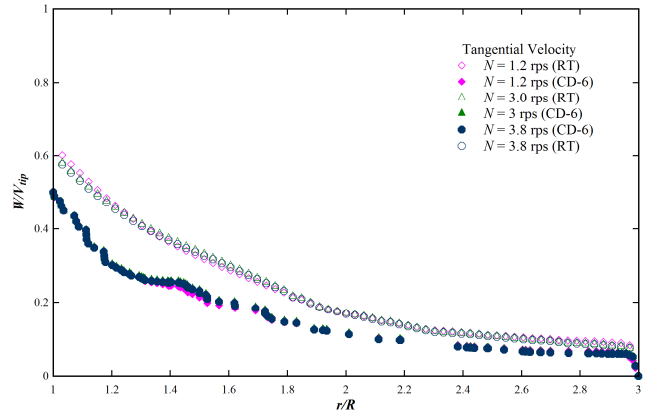

(c) Tangential velocity

Fig. 4 Comparison of predicted velocity components of Rushton turbine and CD-6 impeller

The comparison of impeller discharge velocity profiles of Rushton turbine and CD-6 impeller is shown in Fig. 5. The z^* is non-dimensional axial position and z^* from -1 to +1 represents impeller blade position. All velocity profile data are taken at r/R = 1.1. In Fig. 5 (a), the axial velocity show oscillating outflow profiles. However, the velocity magnitude is higher for Rushton turbine than CD-6 impeller near the impeller blade region. It also observes that the entering and leaving flow velocity magnitude around impeller blade tip region is almost same for CD-6 impeller. While for Rushton turbine, the leaving flow velocity magnitude is higher than the entering flow. From Fig. 5 (a) it is also clear that the Rushton turbine discharge stream angle is slightly higher than the CD-6 impeller. Fig. 5 (b) shows the radial outflow velocity profile. The radial velocity magnitude of CD-6 impeller is higher than Rushton turbine. This can also be concluded from Fig. 3 (b). The velocity magnitude is almost identical for all impeller rotations. While the CD-6 impeller discharges stream shows flatter profile near z^* = 0. The tangential outflow velocity profile is shown in Fig. 5 (c). The width of the profile is larger than the profile of radial velocity profile. This is due to the no-slip condition at impeller surface which enforces the fluid to revolve with impeller blade.

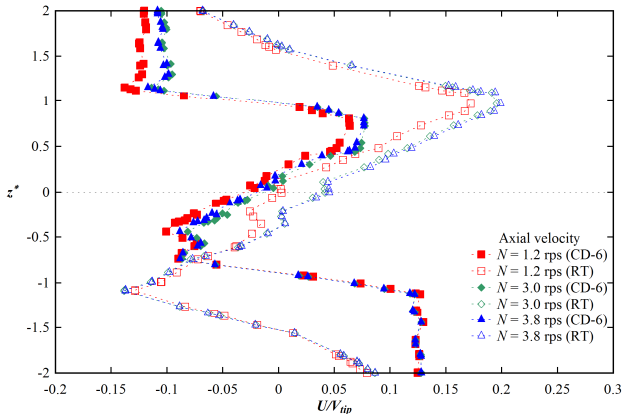

(a) Axial velocity

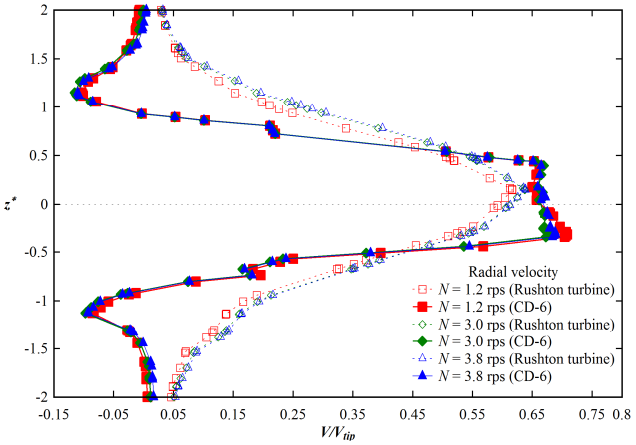

(b) Radial velocity

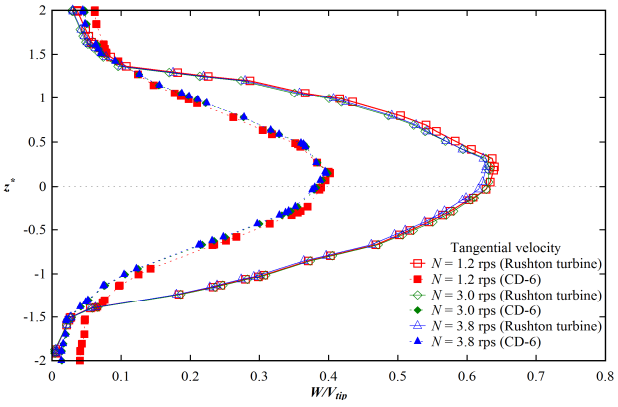

(c) Tangential velocity

Fig. 5 Comparison of impeller discharge velocity components of Rushton turbine and CD-6 impeller

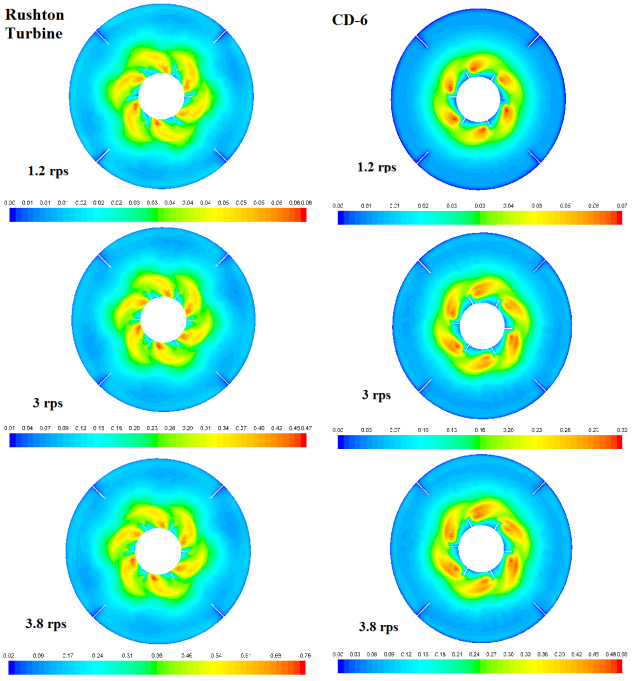

(a) Contours of local turbulent kinetic energy

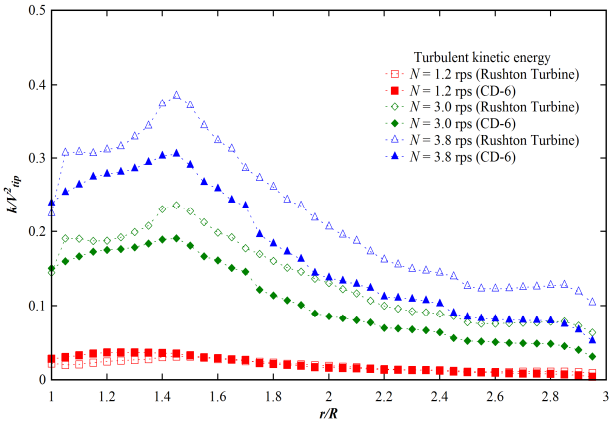

(b) Radial profile of turbulent kinetic energy at H = 0.209m

Fig. 6 Turbulent kinetic energy profile

The turbulent kinetic energy, k, has significant impact on the performance of a stirred tank. The turbulent kinetic energy contours and radial profile at different impeller rotations are shown in Figs. 6 (a) and (b). The maximum magnitude of k is observed near the impeller vicinity. At low rotations, the magnitude of k is almost equal for both Rushton turbine and CD-6 impeller. However, the rotations of impeller increases, the magnitude of k produce by Rushton turbine is higher than CD-6 impeller. The local high value of k in the contours shows the presence trailing vortices produced by the impeller blades. These trailing vortices affect the impeller efficiency. The minimizing the vortex size improves the blending performance of the impeller. The trailing vortices in CD-6 impeller are less elongated and wider than the Rushton turbine. The maximum value of k occurs at r/R = 1.5 for impeller rotation 3 and 3.8 rps is due to the interaction with the trailing vortex from preceding impeller blade.

An accurate CFD simulation should be able to predict the overall power input to the impeller [25]. Fig. 7 shows the power number and flow number curve for CD-6 and Rushton turbine impeller. In turbulent flow regime, Power number of both the impeller is almost constant. The power number for CD-6 impeller and Rushton turbine is about 2.7 and 5 respectively. These values are roughly matched with the literature data for Newtonian fluid [20], [26]. The power requirement of Rushton turbine is nearly twice than CD-6 impeller. The effect of power requirement of impellers can be seen on the flow number. The volume of fluid discharge from the Rushton turbine is about 25% more than CD-6 impeller.

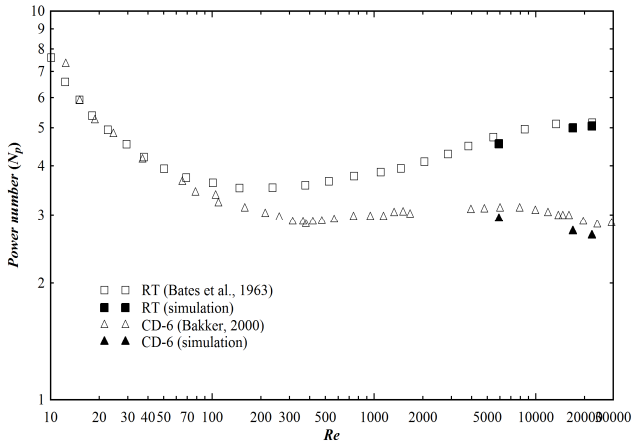

(a)

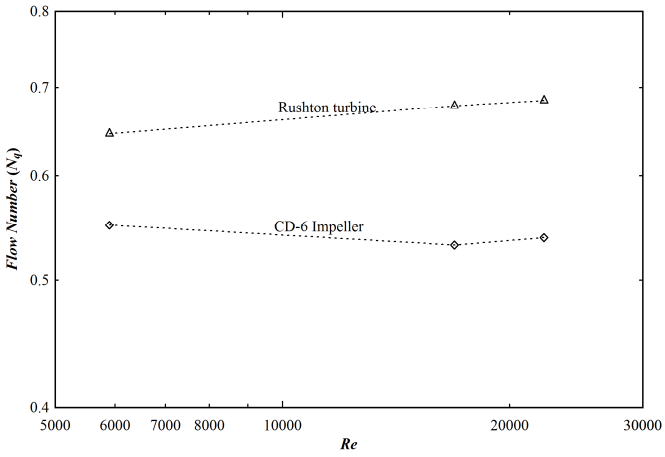

(b)

Fig. 7 (a) Power number curve; (b) Flow number curve

The local viscous dissipation rate contours in the stirred tank is shows in Fig. 8. The viscous dissipation rate is large in the vicinity of impeller and further away from the impeller, the viscous dissipation rate is negligible. The entropy generation due to viscous dissipation rate is shown in Fig. 9. The entropy generation rate for Rushton turbine is higher than the CD-6

impeller at all the Reynolds number. This is due to the consumption of additional power by Rushton turbine which increased viscous loss to stirrer the fluid inside the tank. Thus, the mixing of fluid is increased, but at the expense of more power consumption. However, the system needs to be energy efficient then the CD-6 impeller can be used to stirrer the fluid with reasonable mixing.

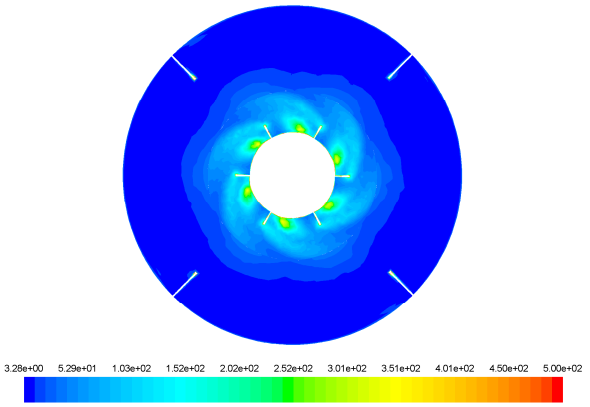

(a) Rushton turbine

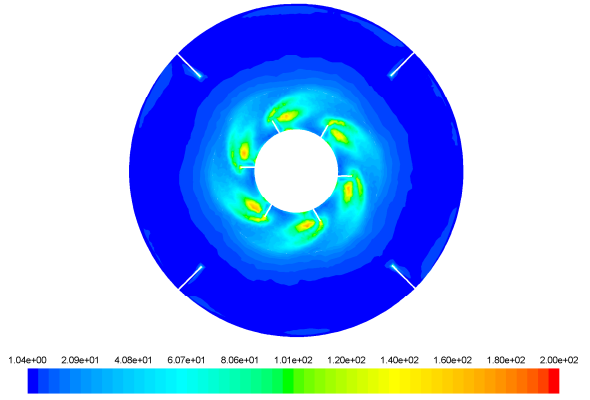

(b) CD-6 impeller

Fig. 8 Contour of local viscous dissipation rate

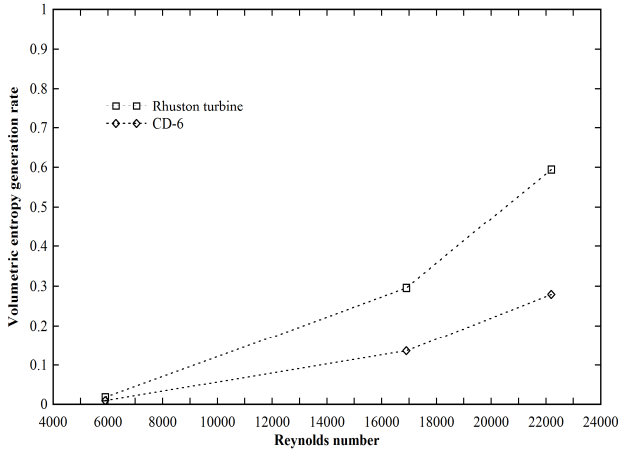

Fig. 9 Volumetric entropy generation rate due to viscous dissipation vs Reynolds number

IV. Conclusions

The comparative study of Rushton turbine and CD-6 impeller is carried out using CFD simulation. The simulation predicted velocity component profiles of Rushton turbine are validated with literature data. The comparative study of hydrodynamics of Rushton turbine and CD-6 impeller is done. The overall velocity magnitude of flow field produce by CD-6 impeller is less than Rushton turbine. However, the radial velocity magnitude near the impeller blade is larger than Rushton turbine. The profiles of turbulent kinetic energy show that the trailing vortices produced by CD-6 impeller are narrow and wider than Rushton turbine. The power number and flow number of CD-6 impeller and Rushton turbine are compared with literature value and it shows the good agreement. The power consumption and entropy generation is less for CD-6 impeller. So, CD-6 impeller can be replaced with Rushton turbine if energy efficiency is prior required.

References

[1] Y. Kawase, K. Shimizu, T. Araki and T. Shimodaira, "Hydrodynamics in three-phase stirred tank reactors with non-Newtonian fluids," Industrial & Engineering Chemistry Research, vol. 36, no. 1, pp. 270–276, 1997.

[2] H. Ameur, M. Bouzit and M. Helmaoui, "Numerical study of fluid flow and power consumption in a stirred vessel with a Scaba 6SRGT impeller," Chemical and Process Engineering, vol. 32, no. 4, pp. 351–366, 2011.

[3] E. Koutsakos and A.W. Nienow, Effects of rheological properties of simulated fermentation broths on flows in stirred bioreactors: A laser anemometry study, Rheology of food, pharmaceutical and biological martials with general rheology, R.E. Carter (ed.), pp. 284–303, 1990.

[4] J. Nouri and J. Whitelaw, "Flow characteristics of stirred reactors with Newtonian and non-Newtonian fluids," AIChE Journal, vol. 36, no. 4, pp. 627–629, 1990.

[5] J. Solomon, T. Elson and A. W. Nienow, "Cavern sizes in agitated fluids with a yield stress," Chemical Engineering Communication, vol. 11, no. 1-3, pp. 143-164, 1981.

[6] B. Venneker, J. Derksen and H. E. A. Van den Akker, "Turbulent flow of shear-thinning liquids in stirred tanks-The effects of Reynolds number and flow index," Chemical Engineering Research and Design, vol. 88, no. 7A, pp. 827–843, 2010.

[7] H. Ameur and M. Bouzit, "Mixing in shear thinning fluids," Brazilian Journal of Chemical Engineering, vol. 29, no. 2, pp. 349–358, 2012.

[8] M. Dular, T. Bajcar, L. Slemenik-Perse, M. Zumer and B. Sirok, "Numerical simulation and experimental study of non-Newtonian mixing flow with a free surface," Brazilian Journal of Chemical Engineering, vol. 23, no. 4, pp. 473–486, 2006.

[9] P. Tanguy, M. Heniche, C. Rivera, C. Devals and K. Takenaka, "Recent developments in CFD applied to viscous and non-Newtonian mixing in agitated vessels," Paper presented at 5th International Conference on CFD in the Process Industries, CSIRO, Melbourne, Australia, 2006.

[10] W. Kelly and B. Gigas, "Using CFD to predict the behaviour of power law liquids near axial-flow impellers operating in the transitional flow regime," Chemical Engineering Science, vol. 58, no. 10, pp. 2141-2152, 2003.

[11] W. Binxin, "CFD investigation of turbulence models for mechanical agitation of non-Newtonian fluids in anaerobic digesters," Water Research, vol. 45, no. 5, pp. 2082-2094, 2011.

[12] S. Masiuk and H. Lacki, "Power consumption and mixing times for Newtonian and non-Newtonian liquids mixing in a ribbon mixer," The Chemical Engineering Journal, vol. 52, no. 1, pp. 13–17, 1993.

[13] J. Netusil and F. Rieger, "Power consumption of screw and helical ribbon agitators in highly viscous pseudoplastic fluids," The Chemical Engineering Journal, vol. 52, no. 1, pp. 9–12, 1993.

[14] M. Ammar, W. Chtourou, Z. Driss, M. S. Abid, "Numerical investigation of turbulent flow generated in baffled stirred vessels equipped with three

different turbines in one and two stage system," Energy, vol. 36, no. 8, pp. 5081–5093, 2011.
[15] N. Dohi, T. Takahashi, K. Minekawa, Y. Kawase, "Power consumption and solid suspension performance of large-scale impellers in gas-liquid-solid three phase stirred tank reactors," Chemical Engineering Journal, vol. 97, no. 2-3, pp. 103–114, 2004.
[16] A. R. Khopkar and P. A. Tanguy, "CFD simulation of gas-liquid flows in stirred vessel equipped with Rushton turbines: influence of parallel, merging and diverging flow configuration," Chemical Engineering Science, vol. 63, no. 14, pp. 3810–3820, 2008.
[17] G. F. Naterer and O. B. Adeyinka, "Magnetic Stirring Tank and Parallel Channel Flow," Entropy, vol. 11, no. 3, pp. 334–350, 2009.
[18] Z. Driss, S. Karray, W. Chtourou, H. Kchaou and M. S. Abid, "A study of mixing structure in stirred tanks equipped with multiple four-blade Rushton impellers," The Archive of Mechanical Engineering, vol. 59, no. 1, pp. 53–72, 2012.
[19] Ansys Fluent 13, Theory Guide, Ansys Inc., U.S.A., 2011.
[20] A. Bakker, A new gas dispersion impeller with vertically asymmetric blades, The Online CFM Book, 2000. http://www.bakker.org/cfm
[21] A. B. Metzner and R. E. Otto, "Agitation of non-Newtonian fluids," AIChE Journal, vol. 3, no. 1, pp. 3-10, 1957.
[22] T. Cebeci and P. Bradshaw, Physical and computational aspects of convective heat transfer, New York: Springer, 1984.
[23] F. Kock and H. Herwig, "Entropy production calculation for turbulent shear flows and their implementation in cfd codes," International Journal of Heat and Fluid Flow, vol. 26, no. 4, pp. 672–680, 2005.
[24] S.V. Patankar, Numerical heat transfer and fluid flow, Series in Computational Methods in Mechanics and Thermal Sciences, Hemisphere, Washington, DC, 1980.
[25] D. Deglon and C. Meyer, "CFD modeling of stirred tanks: Numerical considerations," Minerals Engineering, vol. 19, no. 10, pp. 1059–1068, 2006.
[26] R. L. Bates, P. L. Fondy and R. R. Corpstein, "An examination of some geometrical parameters of impeller power," Industrial & Engineering Chemistry Process Design and Development, vol. 2, no. 4, pp. 310–314, 1963.